Available online at www.sciencedirect.com
SCIENCE DIRECT®
Coordination Chemistry Reviews 248 (2004) 1391–1406
COORDINATION CHEMISTRY REVIEWS
www.elsevier.com/locate/ccr

Review

Cation effects in nanocrystalline solar cells

David F. Watson, Gerald J. Meyer*

Departments of Chemistry and Materials Science and Engineering, Johns Hopkins University, 3400 N. Charles St., Baltimore, MD 21218, USA

Received 27 October 2003; accepted 24 February 2004
Available online 2 July 2004

Contents

Abstract 1391
1. Introduction 1391
2. Single-crystal semiconductors 1392
   2.1. Mechanism of anodic sensitization 1392
   2.2. pH effects on single-crystal metal oxide semiconductors 1393
3. Underivatized nanocrystalline TiO_2 1394
   3.1. Potential distribution within nanocrystalline semiconductor particles: accumulation versus Fermi-level pinning 1394
   3.2. Cation effects on the energetics of nanocrystalline TiO_2 films 1395
   3.3. Carrier transport 1396
4. Dye-sensitized nanocrystalline TiO_2 1397
   4.1. Sensitizer surface-attachment equilibria 1397
   4.2. Energetics of derivatized nanocrystalline semiconductor films 1398
   4.3. Influence of cations on electron injection yields at nanocrystalline metal oxide semiconductors 1398
   4.4. Influence of cations on electron injection dynamics 1402
   4.5. Influence of cations on the kinetics of charge recombination and iodide oxidation 1403
5. Conclusions 1404
Acknowledgements 1405
References 1405

Abstract

Over the past 20 years, the pioneering work of Michael Grätzel and coworkers has led to the development of highly efficient nanocrystalline dye-sensitized solar cells. The energy conversion mechanism of dye-sensitized solar cells involves photoinduced interfacial electron transfer reactions. The cation concentration at the semiconductor/electrolyte interface exerts a profound influence on the mechanism and efficiency of these electron transfer reactions. In this article, we review significant contributions to the understanding of cation effects in nanocrystalline solar cells.

Keywords: Cation effects; Nanocrystalline; Solar cells; Dye-sensitization

1. Introduction

The sensitization of metals and semiconductors to visible light involves interfacial electron transfer following selective excitation of a molecular chromophore. Commonly-studied chromophores, which will be referred to as *dyes* or *sensitizers*, include organic molecules and inorganic complexes. In the 1960s and 1970s, theoretical and experimental studies of dye-sensitized single-crystal semiconductors led to an understanding of the sensitization mechanism [1–6]. However, the development of efficient dye-sensitized solar cells using planar semiconductor electrodes was precluded by poor light harvesting efficiencies and low photocurrent densities.

To increase the light harvesting efficiency, Grätzel and coworkers prepared high surface area, mesoporous, nanocrystalline semiconductor films on conductive glass substrates [7–11]. The effective surface area for sensitizer binding was roughly 1000-fold more than that of a planar electrode. Sensitizer surface coverages of

* Corresponding author. Tel.: +1-4105167319; fax: +1-4105168420.
E-mail address: meyer@jhu.edu (G.J. Meyer).

0010-8545/$ – see front matter © 2004 Elsevier B.V. All rights reserved.
doi:10.1016/j.ccr.2004.02.015

1.3×10^{-7} mol cm^{-2} were achieved, allowing for light harvesting efficiencies of more than 99% from 400 to 550 nm [11]. Sensitization yields were close to unity. Under simulated AM 1.5 solar irradiance conditions, a global energy conversion efficiency of ∼7% was realized in 1991 and has since been optimized to 10.69% [12,13]. Due to their high conversion efficiency and photostability, nanocrystalline dye-sensitized solar cells may represent a practical approach to solar energy conversion.

In their landmark 1991 paper, O'Regan and Grätzel reported that the nature and concentration of cationic species in the electrolyte exerted a profound influence on the efficiency of nanocrystalline dye-sensitized solar cells [11]. Specifically, they measured increased photocurrent with an electrolyte containing lithium iodide relative to an electrolyte containing tetrapropyl ammonium iodide. Their findings have spawned renewed interest in studying cation effects in dye-sensitized photoelectrochemical cells. Cations have been found to affect many parameters that influence solar cell performance, including the strength of sensitizer surface attachment, the energetics of the semiconductor and sensitizer, the charge transport rate, the dynamics of interfacial electron transfer, and the rate of iodide oxidation. In this article, we review significant contributions to the understanding of cation effects in nanocrystalline dye-sensitized solar cells. We begin by reviewing early studies of the influence of proton concentration on the energetics and sensitization efficiency of planar semiconductors. We then cover more recent studies of cation effects in nanocrystalline systems.

2. Single-crystal semiconductors

2.1. Mechanism of anodic sensitization

The accepted mechanism for sensitized anodic photocurrent generation at semiconductor electrodes is outlined in Scheme 1. An excited sensitizer, S*, injects an electron into the semiconductor with rate constant k_{inj}. The oxidized sensitizer accepts an electron from a donor present in the electrolyte, k_{red}. The donor oxidation chemistry is reversed at the dark cathode. Charge recombination, k_{cr}, can occur to the oxidized sensitizer, S^+, or oxidized donor, D^+. Sensitization allows electrical current and voltage to be generated with light of lower energy than the semiconductor bandgap while no net chemistry occurs.

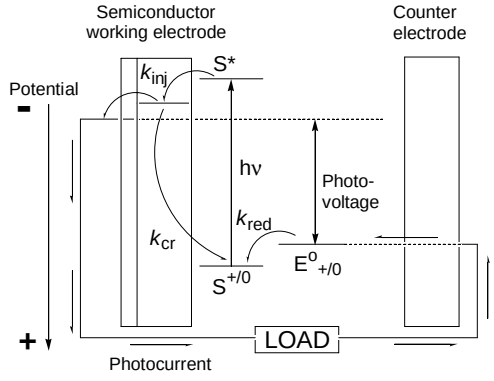

Scheme 1.

The rate of interfacial electron transfer at an electrode surface is proportional to the overlap of occupied donor excited states with unoccupied acceptor states. For electron injection from an excited sensitizer

$$k_{inj} \sim \int \kappa(E) D(E) W_{don}(E)\, dE \quad (1)$$

where $\kappa(E)$ is the transfer frequency, $D(E)$ is the density of unoccupied acceptor states in the semiconductor, and $W_{don}(E)$ is the sensitizer excited-state donor distribution function [1,2]. Fluctuations in the solvation of the sensitizer give rise to a distribution of excited state energies. Gerischer defined the donor and acceptor excited state distribution functions, $W_{don}(E)$ and $W_{acc}(E)$, as follows:

$$W_{don}(E) = \frac{1}{\sqrt{4\pi\lambda k_B T}} \exp\left(-\frac{(E - {}^\circ E)^2}{4\lambda k_B T}\right) \quad (2)$$

$$W_{acc}(E) = \frac{1}{\sqrt{4\pi\lambda k_B T}} \exp\left(-\frac{(E + {}^\circ E)^2}{4\lambda k_B T}\right) \quad (3)$$

where λ is the reorganization energy of interfacial electron transfer, k_B is Boltzmann's constant, T is temperature, E is energy, and E° is the energy of the most probable solvation state [2]. Thus, the rate and efficiency of electron injection from the sensitizer excited state depend on the overlap of the sensitizer excited state distribution function with the density of semiconductor acceptor states (Fig. 1). The sensitizer excited state distribution depends on the reorganization energy for interfacial electron transfer, which is related to the interactions between the sensitizer and its solvation sphere.

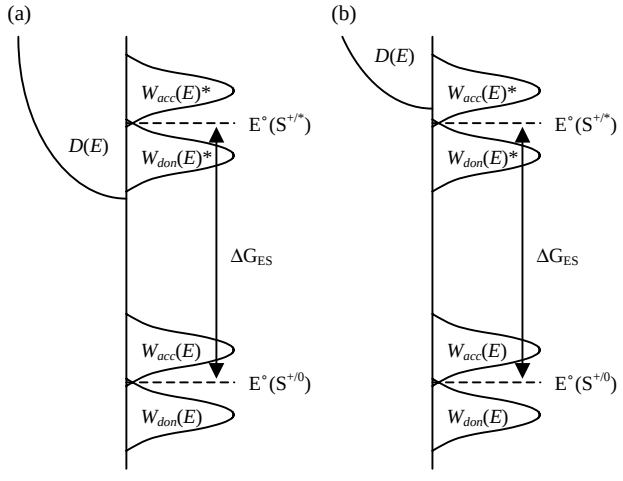

Fig. 1.

2.2. pH effects on single-crystal metal oxide semiconductors

The flatband potential of metal oxide semiconductors in aqueous solution is determined by the proton concentration at the semiconductor–electrolyte interface [14–16]. Watanabe et al. reported capacitance measurements for single-crystal TiO_2 and $SrTiO_3$ [17,18]. Bolts and Wrighton reported similar experiments on single-crystal TiO_2 and SnO_2 [19]. Both groups found that flatband potentials (E_{fb}) exhibited a Nernstian dependence on electrolyte pH, shifting positively with increasing acidity, ~59 mV/pH. This effect has been attributed to protonation/deprotonation equilibria at the semiconductor surface:

$$M-OH \rightleftharpoons M-O^- + H^+ \quad (4)$$

Changes in the interfacial proton concentration induce changes in the surface charge and the potential drop across the Helmholtz layer [16]. The flatband potential is determined by the extent of surface protonation:

$$E_{fb} = E_{fb(pzzp)} - \frac{2.3RT}{F}(pH–pH_{(pzzp)}) \quad (5)$$

where pzzp is the point of zero zeta potential, or zero net surface charge, R is the gas constant, T is temperature, and F is Faraday's constant [16].

The pH-dependence of semiconductor energetics can affect the sensitization efficiency. Movement of the semiconductor flatband potential changes the degree of overlap between the sensitizer excited state distribution function and the density of semiconductor acceptor states, which determines the rate of electron injection, k_{inj} (Eq. (1), Fig. 1). Watanabe et al. were the first to correlate pH-dependent anodic sensitized photocurrents with shifts of the flatband potential [20]. They studied the sensitization of single-crystal TiO_2 with rhodamine B and 3,3′-diethylthiacarbocyanine. A logarithmic dependence of the sensitized photocurrent on electrolyte pH was observed. The effect was attributed to the linear shift of E_{fb} with pH and the resulting changes in the overpotential for interfacial electron transfer.

Clark and Sutin performed similar studies on the sensitization of single-crystal rutile TiO_2 with ruthenium(II) polypyridyl dyes. They studied three dyes with different excited state reduction potentials: $Ru(bpy)_3^{2+}$, $Ru[4,7\text{-}(CH_3)_2\text{-phen}]_3^{2+}$, and $Ru(5\text{-Cl-phen})_3^{2+}$, where bpy is 2,2′-bipyridine and phen is 1,10-phenanthroline [21]. Three- to ten-fold increases of sensitized photocurrent were measured upon acidification of the electrolyte. The pH dependent sensitized photocurrents were attributed to changes in the relative energies of the sensitizer excited states and the TiO_2 acceptor states. As the electrolyte was acidified, the TiO_2 acceptor states shifted to more positive potentials than the sensitizer excited states, increasing the overlap integral and thus the sensitized photocurrent. The pH range through which the photocurrent onsets occurred varied with the reduction potentials of the dyes. For instance, the onset of sensitized photocurrent for $Ru[4,7\text{-}(CH_3)_2\text{-phen}]_3^{2+}$ occurred ~5 pH units more basic than the onset of sensitized photocurrent for $Ru(5\text{-Cl-phen})_3^{2+}$, consistent with the ~250 mV difference in excited state reduction potentials. Clark and Sutin realized that the energetic shift of the TiO_2 acceptor states through the pH range of photocurrent onset (at 59 mV/pH) must be related to the width of the sensitizer excited state distribution functions, $W_{don}(E)$. The reorganization energies for electron injection, λ, were extracted from $W_{don}(E)$ (Eq. (2)). For $Ru[4,7\text{-}(CH_3)_2\text{-phen}]_3^{2+}$, Clark and Sutin reported $\lambda = 0.25$ eV. Sonntag and Spitler subsequently measured

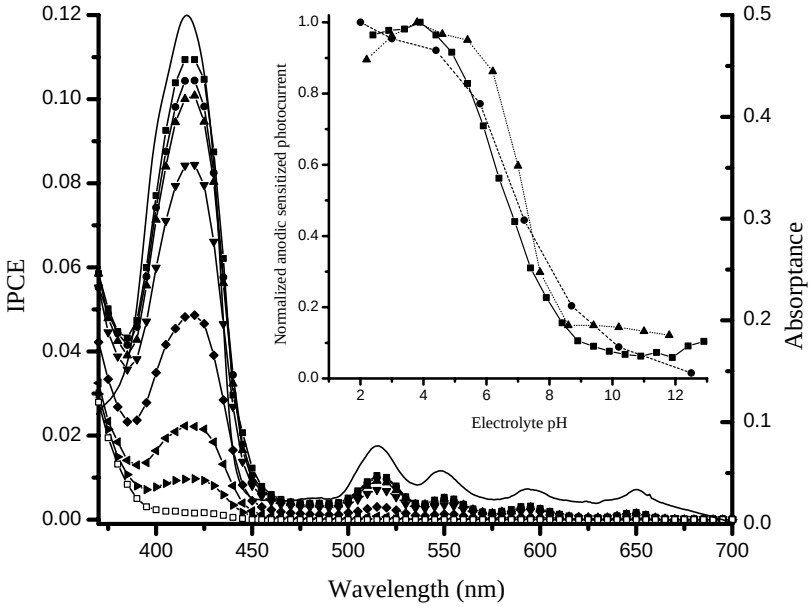

Fig. 2.

pH-dependent photocurrents for $SrTiO_3$ sensitized with the surface-adsorbed organic dyes, 2,2′-diethylthiacarbocyanine and 2,2′-diethyloxadicarbocyanine [22]. They reported reorganization energies of 0.275–0.375 eV and concluded that Gerischer's formulation of interfacial electron transfer applied to surface-adsorbed sensitizers. The work of Watanabe et al., Clark and Sutin, and Sonntag and Spitler clearly showed that electrolyte pH exerts a profound influence on the efficiency of excited state anodic sensitization.

Watson et al. recently reported pH-dependent sensitized photocurrents for porphyrin-derivatized, low surface area TiO_2 films [23]. The singlet excited state reduction potentials of three porphyrin dyes were more than 400 mV negative of E_{fb}, even at basic pHs, where E_{fb} was shifted most negative. In light of the theory outlined above, electron injection was expected to be activationless regardless of the electrolyte pH. Nonetheless, the magnitude of sensitized photocurrent for all three porphyrin sensitizers increased by 10-fold on adjusting the electrolyte pH from 12 to 2 (Fig. 2). Furthermore, plots of photocurrent versus pH were independent of the porphyrin sensitizer, in spite of an ∼650 mV range in excited state potentials (Fig. 2, inset). To rationalize these observations, Watson et al. invoked a mechanism in which a protonated Ti^{IV} surface state is reduced by electron injection from the sensitizer excited state. Protonation is presumably required for charge compensation of the injected electron. These studies reveal that the interfacial proton concentration affects more than just the semiconductor energetics, and that sensitized photocurrent is not necessarily governed only by the thermodynamics for injection.

3. Underivatized nanocrystalline TiO_2

3.1. Potential distribution within nanocrystalline semiconductor particles: accumulation versus Fermi-level pinning

Nanocrystalline semiconductor films exhibit novel behavior that is not observed at planar semiconductors. Before considering cation effects in nanocrystalline films, we briefly discuss their unique electronic properties. Conventional models of the potential distribution at planar semiconductor–electrolyte junctions are not expected to be applicable to nanocrystalline semiconductor films. The potential distribution within the complex three-dimensional semiconductor network is not well understood and represents a major challenge for future photoelectrochemical research. Below we highlight significant contributions from theory and experiments that address some basic issues and have implications for the interfacial electron transfer processes relevant to dye sensitization.

For colloidal materials the small size of the semiconductor particles severely restricts the magnitude of the electric field a particle can support. Albery and Bartlett first considered the potential distribution within spherical semiconductor particles [24]. For large particles, the potential drop across the space-charge layer is equivalent to that for planar electrodes. For small semiconductor particles, the total band bending within the semiconductor, $\Delta\phi_{sc}$, is limited by the radius, r

$$\Delta\phi_{sc} = \frac{k_B T}{6e}\left(\frac{r}{L_D}\right)^2 \tag{6}$$

where e is the charge of an electron and L_D is the Debye length given by Eq. (7):

$$L_D = \sqrt{\frac{\varepsilon_0 \varepsilon k_B T}{2e^2 N_D}} \tag{7}$$

where ε_0 is the permittivity of free space, ε is the dielectric constant of the semiconductor, and N_D is the donor density. The key point is that nanometer-sized semiconductor particles cannot support large electric fields. For example, a 25 nm TiO_2 particle with a relative permittivity of 173 and $N_D = 10^{17}\ cm^{-3}$ is completely depleted at a band bending of only 0.6 meV.

It has been known for some time that electrochemical, chemical, or photoelectrochemical reduction of TiO_2 leads to increased conductivity, blue or black coloration, and paramagnetic behavior. The nature of the states created upon reduction has been the subject of much discussion and debate over the years. In 1986, Heller stated, in response to a question, that TiO_2 reduction yields a "Ti^{III} center or 'state' that adds an electron to the conduction band. To add an electron the state must be either in the band or close to it [25]". It remains unknown whether TiO_2 reduction yields discrete Ti^{III} states or conduction band electrons and how the two possibilities can be unambiguously differentiated. The issue is important when considering interfacial electron transfer and the nature of the redox active states in TiO_2. Some recent literature results that address this issue are described below.

A significant theoretical contribution to the potential distribution within nanocrystalline TiO_2 films was proposed by Rothenberger et al. [26]. They employed a Schottky junction model to derive the potential distribution within TiO_2 particles at negative applied potentials. The model is based on the assumption that an accumulation layer can be created within each nanocrystalline particle as the potential is shifted negative of the flatband potential. They demonstrated, as had others, that an accumulation layer is thinner than a depletion layer when considering cases where the same amount of charge is transferred across the interface. Therefore, in small semiconductor particles an appreciable accumulation layer may be more likely than a depletion layer. Experimentally, a blue–black color, assigned to conduction band and trapped electrons, and a bleach of the fundamental VB → CB absorption, attributed to a Burnstein–Moss shift, were taken as evidence for accumulation layer formation. Spectroelectrochemical analysis, in conjunction with this model, has been used extensively by Fitzmaurice to calculate flatband potentials of nanocrystalline metal oxide films [27–33].

Cao et al. reported an alternative Fermi-level pinning (or band edge unpinning) model to rationalize the potential distribution in nanocrystalline semiconductor particles at negative applied potentials [34]. They pointed out that accumulation layer formation is well known in solid state devices, but that in photoelectrochemical cells Fermi-level pinning with band edge movement has more precedence [35]. Fermi-level pinning refers to the situation where the potential drop across the semiconductor space-charge layer, $\Delta\phi_{sc}$, is fixed, and the potential drop across the Helmholtz layer is variable. Thus, the Fermi level is "pinned" relative to the conduction band edge, which is itself "unpinned". Fermi-level pinning can occur when electroactive surface states or solution phase species are present at the semiconductor–electrolyte interface. When these states are reduced or oxidized, the conduction band edge potential shifts as a result of changes in the Helmholtz layer capacitance.

In principle, capacitance measurements can be used to characterize an accumulation layer and distinguish it from Fermi-level pinning. The potential dependence of the accumulation layer capacitance is given by Eq. (8) [36,37]:

$$C_{sc} \propto \exp\left(\frac{-e\,\Delta\phi_{sc}}{2k_B T}\right) \quad (8)$$

For nanocrystalline anatase TiO_2 films, the accumulation layer capacitance is expected to increase by an order of magnitude for a 120 mV increase in band bending. The 120 mV/decade relationship predicted by Eq. (8) was not realized. Instead a 360 mV/decade relationship was measured, consistent with a significant fraction of the applied potential falling across the Helmholtz layer [34]. Cao et al. suggested that the reduction of localized Ti^{IV} surface states to Ti^{III} pins the Fermi level relative to the conduction band edge potential, and that further increases of applied potential are dropped across the semiconductor–electrolyte interface. Fermi-level pinning is supported by a broad EPR signal at 77 K for electrochemically reduced nanocrystalline TiO_2 films, which was attributed to Ti^{III} species. The existence of trapped electrons in localized Ti^{III} species is also supported by the observation of a maximum at ~1500 nm in the near-IR attenuance spectra of electrochemically reduced nanocrystalline films (free conduction band electrons should exhibit steadily increasing attenuance well beyond 1500 nm [38]). Zaban et al. also found that capacitance data was inconsistent with accumulation layer formation in nanocrystalline TiO_2 films from a sol–gel preparation [39].

The issue of how to characterize reduced TiO_2 remains a subject of debate in the literature. Accurately distinguishing between accumulation and Fermi-level pinning is difficult. The blue–black coloration of reduced nanocrystalline TiO_2 films is consistent with both mechanisms, and important factors such as TiO_2 particle size and the density of surface states vary with changes in the sol–gel preparation technique. Thus, conclusive evidence for the TiO_2 reduction mechanism may not be forthcoming.

3.2. Cation effects on the energetics of nanocrystalline TiO_2 films

Regardless of the mechanism of TiO_2 reduction, determining the potential of the acceptor states that are reduced by interfacial electron injection is important with regard to understanding the energetics and mechanism of sensitization. Space-charge capacitance measurements are often used to determine the flatband potentials of single-crystal semiconductor electrodes. This approach is not useful for nanocrystalline films, however, because particles with 10–20 nm diameters cannot support significant depletion layers. Instead, spectroelectrochemical measurements have proven useful in measuring the energetics of nanocrystalline semiconductor films.

Fitzmaurice and coworkers have calculated flatband potentials of nanocrystalline metal oxide films using spectroelectrochemical measurements and the accumulation layer model [27–33]. They have studied the effects of proton and cation concentration on flatband potentials in aqueous and nonaqueous solvents. Values of E_{fb} were determined from the linear region of absorbance change versus applied potential data. E_{fb} of nanocrystalline TiO_2 films shifted −60 mV/pH in aqueous electrolytes, as anticipated for metal oxide semiconductors [26]. E_{fb} was found to be significantly more positive for water and nonaqueous protic solvents than for nonaqueous aprotic solvents [29]. Addition of trace amounts of water to nonaqueous aprotic solvents resulted in large positive shifts of E_{fb}. Enright et al. measured a linear relationship between E_{fb} and pK_s, the autoprotolysis constant, for four solvents, with E_{fb} shifting positively with decreasing pK_s [31]. These findings are all consistent with a mechanism where E_{fb} is determined by protonation/deprotonation equilibria at the TiO_2 surface.

In basic aqueous electrolytes or nonaqueous aprotic electrolytes with $pK_s < 10^{-17}$, other cations were found to be potential-determining [29,33]. Redmond and Fitzmaurice reported that E_{fb} of nanocrystalline TiO_2 films shifted positively by up to 1.0 V upon addition of 0.1 M $LiClO_4$, $NaClO_4$, or $Mg(ClO_4)_2$ to acetonitrile electrolytes. For a given cation activity, the magnitude of the positive shift of E_{fb} decreased in the order $Mg^{2+} > Li^+ > Na^+$. Cation adsorption and intercalation were proposed as the mechanism by which cations are potential-determining in aprotic solvents.

Hupp and coworkers provided definitive evidence that cation adsorption and/or intercalation are associated with TiO_2 reduction. Using electrochemical quartz crystal microbalance (EQCM) measurements, they observed mass increases of nanocrystalline metal oxide films upon electrochemical or photochemical reduction [40–42]. Reversible mass increases for H^+, D^+, Li^+, and Na^+ were attributed to cation intercalation, while irreversible mass increases for tetrabutylammonium were attributed to cation adsorption. The cation uptake coincided with the growth of a near-IR band in reflectance spectra. Charge compensation of

electron density in the TiO_2 film was cited as the driving force for cation intercalation. Lemon and Hupp argued that the adsorption or intercalation of cations implies that there is local electroneutrality throughout the film, and therefore no potential gradient across the film. Thus, the potential must drop on the solution side of the film, corresponding to Fermi-level pinning rather than accumulation layer formation [42]. Lyon and Hupp reported a Nernstian shift of the TiO_2 conduction band edge potential, E_{cb}, over a log(proton activity) range of 31 pH units [43]. Reversible proton intercalation accompanied TiO_2 reduction over the entire log(proton activity) range. They proposed a mechanism in which E_{cb} is determined by the proton-coupled reduction and oxidation of localized $Ti^{IV/III}$ trap states.

In summary, the findings of Fitzmaurice and Hupp and their coworkers are consistent with a mechanism by which cation adsorption/desorption or intercalation/deintercalation equilbria determine the potential of electrons in nanocrystalline TiO_2. The magnitude of the effect depends on the solvent and the charge-to-radius ratio of the cation. The influence of cation concentration on nanocrystalline TiO_2 energetics exerts a profound effect on the efficiency of anodic sensitization, as discussed in Section 4.

3.3. Carrier transport

Charge carrier transport in a semiconductor film can be described by the continuity equation

$$\frac{\partial n}{\partial t} = \frac{1}{e}\frac{\partial J}{\partial x} + G - R \tag{9}$$

where n is the electron density under illumination, J is the current density in the film, and G and R are the carrier generation rate and recombination rate, respectively [44]. Recombination is assumed to be proportional to the electron concentration and can be written as $R = (n - n_0)/\tau_0$, where n_0 is the electron density in the dark and τ_0 is the position-independent electron lifetime. Both electron drift and diffusion can contribute to the current density:

$$J = en\mu_n \frac{\partial \phi_{sc}}{\partial x} + eD\frac{\partial n}{\partial x} \tag{10}$$

where μ_n is the electron mobility and D is the diffusion coefficient of the electron. In nanocrystalline TiO_2 films, the current density is dominated by the diffusion term. Because the electrolyte permeates throughout the TiO_2 film, charges are screened and electrical neutrality is maintained across the film. Individual TiO_2 particles are too small to sustain significant band bending. Therefore, potential gradients within the film are minimal, and charge transport occurs by diffusion rather than migration.

In the absence of migration, the continuity equation is given by

$$D\frac{\partial^2 n(x,t)}{\partial x^2} - \frac{\partial n(x,t)}{\partial t} - \frac{n(x,t) - n_0}{\tau_0} + \phi\alpha\exp(-\alpha x) = 0 \tag{11}$$

where ϕ is the incident light intensity, α is the reciprocal absorption length, and x is the width of the depletion layer. The first two terms represent the electron flux and the change in electron concentration with time, respectively. The third term represents the recombination rate. The fourth term is the rate of electron generation from injection, which assumes the dye concentration is uniform throughout the film. Eq. (11) has been solved analytically. Södergren and coworkers showed that steady-state photocurrent and photovoltage measurements were consistent with this model and the assumption that electron transport occurs by diffusion [45]. They derived expressions that accurately modeled photocurrent action spectra and current–voltage data with illumination at the TiO_2/electrolyte and substrate/TiO_2 interfaces.

The first time-resolved photocurrent measurements of sensitized nanocrystalline TiO_2 materials were made by Schwarzburg and Willig [46]. They used Shockley–Read kinetics to numerically simulate their data. Photocurrent rise and decay times were fastest with high incident light intensities. Based on the intensity dependence of photocurrent transients, Schwarzburg and Willig concluded that the occupancy of deep trap states influenced the kinetics of electron transport through nanocrystalline TiO_2 films following electron injection.

Cao et al. reported the first transient photocurrent measurements obtained in the frequency domain using intensity modulated photocurrent spectroscopy (IMPS), and compared them to data acquired in the time domain [47]. A characteristic feature of the dye-sensitized porous nanocrystalline TiO_2 photoelectrochemical cells was the appearance of slow photocurrent transients with rise times varying from milliseconds to seconds depending on the experimental conditions. The photocurrent rise time, $t_{1/2}$, which is the time required for the photocurrent to reach half the saturation value, displayed a power law dependence on light intensity with a slope of -0.7. Several considerations led to the conclusion that the slow response was due to the transport of charge in the semiconductor. First, the photocurrent rise times were at least six orders of magnitude slower than the time scale for electron injection. Second, sensitizer regeneration by iodide electrolyte was known to occur rapidly and only contribute to the observed transients at low concentrations or high irradiance. Therefore, the sluggish photocurrent transients were attributed to slow carrier transport. Cao et al. estimated an upper limit for the dark electron diffusion coefficient of $10^{-7}\,cm^2\,s^{-1}$, which is significantly slower than diffusion in the conduction band of single-crystal rutile TiO_2. Based on an electron mobility of about $1\,cm^2\,V^{-1}\,s^{-1}$, the diffusion coefficient for free conduction band electrons determined from the Einstein equation is on the order of $10^{-2}\,cm^2\,s^{-1}$ at room temperature. Cao et al. attributed the slow, intensity-dependent electron transport kinetics to a mechanism in which diffusion is limited by thermal excitation from trap states.

In the past several years, a number of researchers have reported experimental and theoretical studies of electron

transport in nanocrystalline TiO_2 films. Electron transport has been characterized by measurements of transient photocurrent [48–61], transient photovoltage [51,56], intensity-modulated photocurrent spectroscopy (IMPS) [62–64] and intensity-modulated photovoltage spectroscopy (IMVS) [64,65]. Theoretical studies have focused on random walk simulations of electron diffusion [49,50,66,67]. These studies have led to the general acceptance of a mechanism in which charge transport occurs by the thermally-activated diffusion of electrons between trap states. The rate of electron transport is determined by the rates of trapping and detrapping. The factors governing electron transport kinetics are complex. The electron diffusion coefficient has been found to depend on the incident light intensity, film thickness and porosity, TiO_2 particle size and crystallinity, and electrolyte composition. Electron diffusion coefficient values ranging from 10^{-4} to 10^{-8} $cm^2\ s^{-1}$ have been reported.

Kopidakis et al. invoked an ambipolar diffusion mechanism to describe charge transport in nanocrystalline TiO_2 films [48]. They argued that electron transport in TiO_2 is coupled to cation transport in the electrolyte, which permeates throughout the TiO_2 film. The ambipolar diffusion coefficient, D_{amb}, is given by

$$D_{amb} = \frac{n + p}{(n/D_p) + (p/D_n)} \quad (12)$$

where n and p are the electron and cation densities, and D_n and D_p are the electron and cation diffusion coefficients. Under typical experimental conditions, where $n \ll p$, D_{amb} is approximately equal to D_n. Kopidakis et al. reported intensity-dependent ambipolar diffusion coefficients ranging from 10^{-8} $cm^2\ s^{-1}$ at low light intensity to 10^{-4} $cm^2\ s^{-1}$ at high light intensity.

Nakade et al. provided compelling evidence for the validity of the ambipolar diffusion model [56]. Measured values of D_{amb} were independent of light intensity at low electrolyte ion concentrations, but were intensity-dependent at high concentrations. Eq. (12) predicts that D_{amb} approaches D_p when $n \gg p$, and D_{amb} approaches D_n when $p \gg n$. Because diffusion of cationic species in the electrolyte is independent of light intensity, while trap-mediated diffusion of electrons through the TiO_2 film is intensity-dependent, the findings of Nakade et al. are consistent with the ambipolar diffusion model. The influence of the electrolyte cation concentration on the ambipolar diffusion coefficient is the most pronounced effect of cations on charge transport.

Yanagida and coworkers recently reported an in-depth study of cation effects on the electron transport properties of underivatized nanocrystalline TiO_2 films [57]. Ambipolar diffusion coefficients were determined by transient photocurrent measurements in ethanol and acetonitrile electrolytes with varying compositions. For a given electrolyte composition, D_{amb} increased with light intensity. Photocurrent maxima and photogenerated charge densities increased in the order dimethylhexylimidazolium (DMHI) < tetrabutylammonium (TBA^+) < Na^+ < Li^+. For each cation, D_{amb} increased by several orders of magnitude with increasing cation concentration. Transient photocurrent data for TBA^+ and low concentrations of Li^+ and Na^+ were accurately modeled by Eq. (12). At high concentrations of Li^+ and DMHI (>10^{20} cm^{-3}), significant increases of the diffusion coefficient were explained by cation adsorption and its effect on surface trap states.

In summary, charge transport in nanocrystalline TiO_2 films is well modeled by ambipolar diffusion. Under normal experimental conditions, the cation density is much greater than the electron density, and the ambipolar diffusion coefficient is approximately equal to the electron diffusion coefficient. Diffusion coefficients ranging from 10^{-8} to 10^{-4} $cm^2\ s^{-1}$ have been reported. Charge transport kinetics depend strongly on experimental conditions, such as the incident light intensity, the nature of the TiO_2 film, and the electrolyte composition.

4. Dye-sensitized nanocrystalline TiO_2

The influence of cations on semiconductor energetics, as discussed above, profoundly affects many factors that determine solar cell performance, including sensitizer adsorption–desorption equilibria, sensitizer and semiconductor energetics, and the dynamics of interfacial electron transfer. Nanocrystalline semiconductor films are highly transparent in the visible region, allowing interfacial electron transfer processes to be characterized by transmission-based spectroscopic methods and photoelectrochemical techniques. Below we summarize experimental studies that have contributed significantly to the development of an understanding of cation effects on dye-sensitized nanocrystalline solar cells.

4.1. Sensitizer surface-attachment equilibria

In early studies on dye-sensitization of nanocrystalline TiO_2 films, Grätzel and coworkers observed that the surface binding equilibria of organic and inorganic chromophores were influenced by the pH of aqueous adsorption solutions [7,68,69]. Surface attachment through hydroxyl and carboxylic acid functional groups was strong in neutral and acidic solutions, but the dyes desorbed at basic pHs. The pH-dependence of sensitizer adsorption has been utilized to measure surface coverages [12,70–72]. Sensitizer-derivatized films were immersed in basic solutions leading to complete desorption. The amount of dye originally adsorbed on the TiO_2 film was quantified by determining the concentration of desorbed dye in the basic solution.

Qu and Meyer studied the influence of interfacial proton concentration on the binding mode of ruthenium(II) polypyridyl dyes anchored to TiO_2 through carboxylic acid functional groups [73]. Infrared transmission spectra revealed that TiO_2 surfaces pretreated with pH 11 NaOH

exhibited a "carboxylate" binding mode (C–O bond order of 1.5), while TiO_2 surfaces pretreated with pH 1 H_2SO_4 exhibited a "carboxylic acid" binding mode (C–O bond order of 2). The desorption of sensitizers in basic aqueous solutions may be explained by the largely ionic nature of the carboxylate binding mode.

4.2. Energetics of derivatized nanocrystalline semiconductor films

The energetics of surface-bound sensitizers can be affected by the cation concentration at the semiconductor–electrolyte interface. Zaban et al. used chemical redox titrations to measure the potential of inorganic and organic sensitizers bound to TiO_2 [74,75]. These studies revealed that molecular reduction potentials that are pH-independent in aqueous solution can become pH-dependent when the molecule is bound to the semiconductor surface. The pH-induced shifting of reduction potentials varied from 21 to 53 mV/pH depending on the distance of the sensitizer from the semiconductor surface. The reduction potentials of sensitizers lying within the semiconductor double layer tracked the ~59 mV/pH shift of the semiconductor conduction band edge potential. The reduction potentials of sensitizers lying outside of the double layer were nearly pH-independent. These findings have important implications with regard to optimizing the thermodynamics of the electron injection and recombination reactions.

As described above, the energetics of underivatized metal oxide semiconductors are determined by the nature and concentration of cations at the semiconductor–electrolyte interface. Yan and Hupp reported the first measurements of cation-dependent energetics of sensitizer-derivatized nanocrystalline TiO_2 films [76]. Flatband potentials were determined from the onset potential for decreased near-IR laser reflectance. E_{fb} shifted ~60 mV/pH and was roughly 100 mV positive of previously-reported E_{fb} values for underivatized nanocrystalline TiO_2. Thus, sensitizer adsorption exerts a minimal effect on TiO_2 energetics.

4.3. Influence of cations on electron injection yields at nanocrystalline metal oxide semiconductors

As discussed above, the work of Watanabe et al., Clark and Sutin, and Sonntag and Spitler has demonstrated quite convincingly that the photocurrent efficiency can be controlled by pH [20–22]. At low pH, photocurrents were maximized while at high pH no sensitized current was measured, implying that injection was shut off. Unfortunately, many sensitizers bound to metal oxide surfaces through carboxylate linkages desorb at basic pHs, making pH-dependent electron injection studies difficult.

An alternative approach involves studying cation effects in nonaqueous environments. O'Regan and Grätzel were the first to report cation-dependent photoelectrochemical behavior for nonaqueous dye-sensitized nanocrystalline solar cells [11]. They measured incident photon-to-current efficiencies (IPCEs) of 68% with a tetrapropylammonium iodide electrolyte and 84% with a lithium iodide electrolyte. Liu et al. subsequently studied the influence of cations on photocurrent and photovoltage [77]. For alkali iodide electrolytes, the photocurrent decreased and the photovoltage increased with increasing cationic radius. The global efficiencies of solar cells were relatively independent of the cation, due to the tradeoff between photocurrent and photovoltage. Liu et al. attributed the influence of cations on current and voltage to a thermodynamic effect. They argued that smaller cations bind more efficiently to the TiO_2 surface, leading to more positive TiO_2 acceptor state potentials and a greater driving force for injection, but also a lower open-circuit photovoltage.

Meyer and coworkers have since reported kinetic studies of the influence of cations on the excited-state deactivation of surface-adsorbed ruthenium polypyridyl complexes [78]. Photocurrent generation in dye-sensitized nanocrystalline solar cells involves excited state interfacial electron transfer. It is therefore desirable to have a mechanistic understanding of excited state behavior on semiconductor surfaces. Molecular excited states are known to be sensitive to environment, and dramatic changes in lifetimes, quantum yields, and spectral distribution can arise from so-called "rigidochromic" effects observed in insulating solid state materials [79]. Obtaining mechanistic information on the excited states of surface-attached dyes is further complicated by interfacial electron transfer, which rapidly depletes the excited states under many conditions. The weak photoluminescence (PL) that remains has been studied by many groups and has been the subject of a recent review [80]. The difficulty with PL measurements, however, is that the observed PL may stem from a small fraction of the surface-bound compounds that does not represent the ensemble average.

An alternative approach to studying cation effects has been reported by Kelly et al. [78,81]. They determined electron injection yields from transient absorption measurements, and found that the efficiency of electron injection for sensitizer-derivatized nanocrystalline TiO_2 films can be widely "tuned" by varying the electrolyte composition. We first discuss the excited-state decay kinetics of $Ru(bpy)_2(dcb)^{2+}$-derivatized nanocrystalline TiO_2 films in the absence of cations, where dcb = 4,4′-(CO_2H)-2,2′-bipyridine. Fig. 3 shows transient absorbance difference spectra of $Ru(bpy)_2(dcb)^{2+}/TiO_2$ in neat acetonitrile after excitation at 532 nm (~7 ns pulsewidth) [81]. The spectra are consistent with the MLCT excited state of the sensitizer, with an absorption maximum at 380 nm, the bleach of the ground state MLCT transition at 475 nm, and a longer wavelength absorbance beyond 530 nm (the apparent bleach at 650 nm is due to luminescence, which exhibits the same kinetics as the absorbance changes). The rate of transient absorbance changes at 380 and 475 nm corresponds to the kinetics of excited-state deactivation. The nonzero amplitude of the ground/excited state isosbestic point at 403 nm

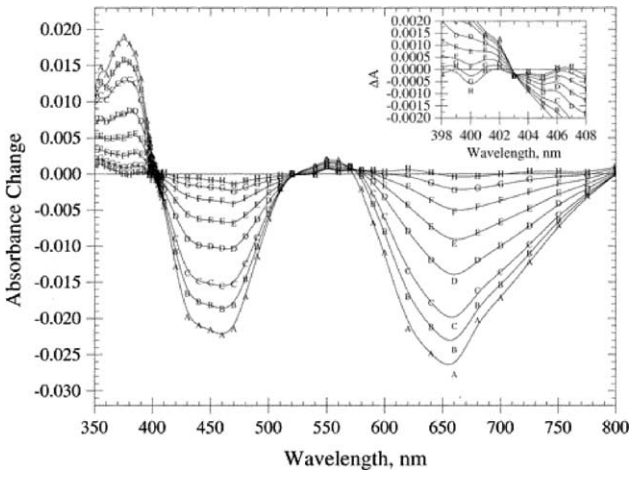

Fig. 3.

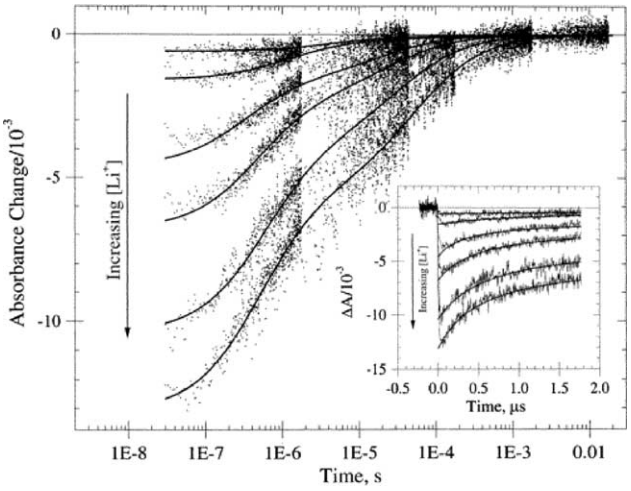

Fig. 4.

has been attributed to the formation of the oxidized sensitizer, which is minimal in neat acetonitrile. By probing the absorbance change at the ground/excited state isosbestic point, the concentration of oxidized sensitizer can be directly measured, without interference from the excited state.

The excited-state decay kinetics of $Ru(bpy)_2(dcb)^{2+}/TiO_2$ films immersed in neat acetonitrile, monitored at 380 and 475 nm, were dependent on the excitation intensity. At low excitation irradiance, near-exponential kinetics were observed. However, at high excitation irradiance, second-order equal concentration kinetics fit the experimental data well. These observations are consistent with competitive first- and second-order processes, attributed to radiative and nonradiative excited-state deactivation (Eq. (13)) proceeding in parallel with excited state annihilation (Eq. (14)).

$$\frac{{}^*Ru(bpy)_2(dcb)^{2+}}{TiO_2} \rightarrow \frac{Ru(bpy)_2(dcb)^{2+}}{TiO_2} + (h\nu \text{ or } \Delta) \quad (13)$$

$$\frac{2[{}^*Ru(bpy)_2(dcb)^{2+}]}{TiO_2} \rightarrow \text{Products} \quad (14)$$

A second-order contribution to the excited state decay of $Ru(bpy)_3{}^{2+}$ adsorbed on surfactant or polymer modified nanocrystalline TiO_2 films has been reported by Rabani et al. [82]. The implied parallel first- and second-order kinetic model has successfully been used to fit many excited state decays on nanocrystalline thin films in our laboratory. The possibility that the first- and second-order rate constants, obtained from fitting kinetic data to this model, represent an underlying distribution of rate constants cannot be ruled out. However, such distributions were not required to fit the data with self consistent rate constants.

Kelly et al. studied the influence of cations on the excited-state deactivation kinetics of $Ru(bpy)_2(dcb)^{2+}/TiO_2$ [78]. Electron injection yields were determined by monitoring time-resolved absorbance changes at the ground/excited state isosbestic point. Increasing the concentration of $LiClO_4$ in the external acetonitrile electrolyte resulted in parallel increases in the yields of electron injection and static PL quenching (i.e. quenching within the ~10 ns instrument response time). Representative transient absorbance data are shown in Fig. 4. These observations are consistent with ultrafast electron injection, which is expected to deplete the excited state concentration and increase the oxidized sensitizer concentration within the 7 ns laser pulse. Remarkably, the injection yield could be reversibly controlled by varying the Li^+ concentration. Both the injection yield and the static PL quenching yield increased with log[Li^+]. Other cations were found to exert a similar influence on the injection yield. The magnitude of the effect varied with the charge-to-radius ratio of the cation, with $Ca^{2+} > Sr^{2+} \sim Ba^{2+} > Li^+ > Na^+ > K^+ = Rb^+ \sim Cs^+ \sim$ tetrabutylammonium (TBA^+) > neat CH_3CN.

Dynamic quenching, or an increase in the rate of excited-state decay, was observed concomitantly with the static quenching. Dynamic quenching has previously been used as an indirect measurement of the electron injection rate. However, the dynamic quenching kinetics with added Li^+ were not paralleled by an increase in the concentration of oxidized sensitizer. Therefore, the enhanced decay rate could not be accounted for by electron injection from the thermally-equilibrated ^{3}MLCT excited state. It was proposed that the dynamic luminescence decay was due to oxidative quenching of the excited state by oxidized sensitizers.

Kelly et al. attributed the cation-dependent electron injection yield to a thermodynamic effect, in which cation adsorption induces a positive shift of TiO_2 acceptor states, resulting in more favorable energetics for electron injection [78]. This thermodynamic argument is consistent with previously-reported interpretations of pH-dependent sensitized photocurrents at single-crystal metal oxide semiconductors [20–22]. Spectroelectrochemical measurements

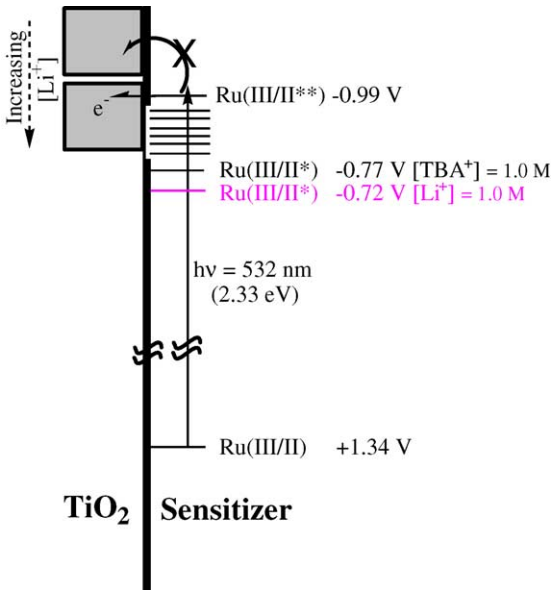

Fig. 5.

indicate that increasing the Li^+ concentration from 0 to 1 M lowers E_{cb} by more than 1 eV and promotes electron transfer from the excited state [29,31]. The thermally-equilibrated ^{3}MLCT excited-state potential is more positive than TiO_2 acceptor state potentials, even at high Li^+ concentrations. Therefore, Kelly et al. proposed that electron injection occurs from vibrationally-excited MLCT states, prior to thermalization to the vibrationally-relaxed ^{3}MLCT state. Electron injection from vibrationally "hot" excited states is consistent with the observed ultrafast injection and static PL quenching. The mechanism for cation-controlled electron injection yields is summarized in Fig. 5.

The photoelectrochemical behavior of $Ru(bpy)_2(dcb)^{2+}$/TiO_2 was consistent with the mechanism described above. Under white light excitation, the short-circuit photocurrent was ~3.5 times greater with a LiI-containing electrolyte than with a TBAI-containing electrolyte. The open-circuit photovoltage was significantly lower for LiI than for TBAI. These findings were in agreement with the results of O'Regan and Grätzel and Liu et al. [11,77]. The increased short-circuit photocurrent is reasonable in light of the increased injection yield, while the decreased open-circuit voltage is consistent with a positive shift of TiO_2 acceptor state potentials with increasing Li^+ concentration.

Cation-dependent excited-state electron injection yields have been investigated in a variety of systems in our laboratory. The ability to control the electron injection efficiency by adjusting the electrolyte cation concentration is a powerful tool for altering the reactivity of surface bound sensitizers. In several of the following examples, the dependence of excited-state injection yield on the interfacial cation concentration enables systematic control over the mechanism and efficiency of electron transfer and energy transfer processes at the semiconductor surface.

Farzad et al. reported competitive intermolecular energy transfer and interfacial electron injection on nanocrystalline TiO_2 films derivatized with co-adsorbed $Ru(bpy)_2(dcb)^{2+}$ and $Os(bpy)_2(dcb)^{2+}$ [83]. When the films were immersed in neat acetonitrile, efficient intermolecular energy transfer from excited $Ru(bpy)_2(dcb)^{2+}$ to $Os(bpy)_2(dcb)^{2+}$ was observed ($\phi_{en} \sim 1$), Eq. (15).

$$Ru(dcb)(bpy)_2{}^{2+*} + Os(dcb)(bpy)_2{}^{2+} \xrightarrow{k_{en}} Ru(dcb)(bpy)_2{}^{2+} + Os(dcb)(bpy)_2{}^{2+*} \quad (15)$$

Addition of $LiClO_4$ to the external acetonitrile solution lowered the energy transfer yield and promoted interfacial electron injection. The effect was attributed to positive shifts of TiO_2 acceptor states. The energy transfer yield could be reversibly turned on and off by alternating between neat acetonitrile and 1.0 M $LiClO_4$.

Thompson et al. and Bergeron and Meyer reported an alternative electron injection mechanism, in which injection occurs from the reduced sensitizer rather than the sensitizer excited state [84,85]. Transient absorption measurements revealed that both injection mechanisms were operative for $Ru(bpy)_2(deeb)^{2+}$-sensitized nanocrystalline TiO_2, where deeb is 4,4′-diethylester-2,2′-bipyridine. The relative efficiencies of electron injection from the reduced and excited sensitizer depended on the concentration of $LiClO_4$ in an external acetonitrile solution containing phenothiazine, PTZ. At high Li^+ concentrations, excited-state injection predominated, while at low Li^+ concentrations, injection from the reduced sensitizer was favored. This effect was explained in terms of Li^+-induced energetic shifts of TiO_2 acceptor states. Reductive quenching of the $^*Ru(bpy)_2(deeb)^{2+}$ excited state by PTZ yielded $[Ru(bpy)_2(deeb^-)]^+$. The redox potential of ($deeb^-$) is roughly 400 mV more negative than that of the thermally-equilibrated excited state, $^*Ru(bpy)_2(deeb)^{2+}$. Therefore, the driving force for electron injection from the reduced sensitizer is significantly greater than for injection from the excited sensitizer (Fig. 6). In the absence of Li^+, TiO_2 acceptor states are shifted to relatively negative potentials, and injection from $^*Ru(bpy)_2(deeb)^{2+}$ is prohibited while injection from $Ru(bpy)_2(deeb^-)^+$ is thermodynamically favorable. At high Li^+ concentrations, injection from $^*Ru(bpy)_2(deeb)^{2+}$ becomes favorable, and excited-state injection, an ultrafast process, predominates over sensitizer reduction by PTZ.

Yang et al. reported the first compounds capable of sensitization by both direct electron injection and excited-state injection [86,87]. Direct electron injection, or metal-to-particle charge-transfer (MPCT), proceeds by photoinduced interfacial electron transfer from a sensitizer ground state to a semiconductor acceptor state, Eq. (16).

$$\frac{S}{TiO_2} \xrightarrow{h\nu} \frac{S^+}{TiO_2(e^-)} \quad (16)$$

MPCT is well known for ferrocyanide-derivatized TiO_2 [88,89]. The UV-Vis absorption spectra of $Fe(LL)(CN)_4{}^{2-}$/

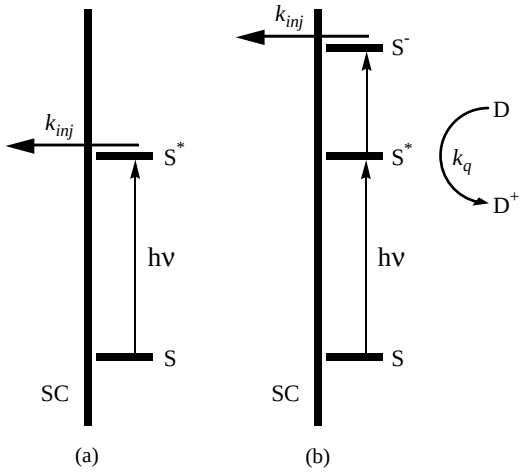

Fig. 6.

TiO_2, where LL = bpy, 4,4′-dimethyl-2,2′-bipyridine (dmb), or 4,4′-diphenyl-2,2′-bipyridine (dpb), were accurately fit by the sum of two Gaussians, corresponding to Fe(II) → LL MLCT and Fe(II) → TiO_2 MPCT bands [86,87]. The overall electron injection yields, and the relative yields of MPCT and excited-state injection, depended on the concentration of Li^+ in the external acetonitrile electrolyte. Cation-dependent injection yields necessarily imply that the excited-state injection mechanism was operative, because direct injection by definition must have a quantum yield of unity. The increased excited-state injection yield at high Li^+ concentrations was assigned to the movement of TiO_2 acceptor states to more positive potentials than the MLCT excited state.

Stux and Meyer recently reported a wavelength-ratiometric method for sensing calcium ions based on cation-dependent PL quenching yields [90]. The addition of Ca^{2+} to the external acetonitrile solution induced a red shift and quenching of emission intensity from $^*Ru(bpy)_2(deeb)^{2+}/TiO_2$. Static and dynamic quenching were observed. A linear relationship was measured between the Ca^{2+} concentration and the ratio of PL intensities at 654 and 684 nm (PLI_{654}/PLI_{684}). This wavelength-ratiometric sensing technique was sensitive to $\sim 10^{-8}$ M Ca^{2+} concentrations, and was much more reliable than intensity and lifetime-based sensing methods.

Recent studies have demonstrated that the cation effects discussed above are not limited to anatase nanocrystalline TiO_2. Park et al. have reported cation-dependent photocurrent and photovoltage in dye-sensitized nanocrystalline rutile TiO_2 solar cells [91]. The short-circuit photocurrent with a lithium iodide electrolyte was roughly 25% greater than with a 1,2-dimethyl-3-hexyl imidazolium iodide electrolyte. The reverse trend was observed in photovoltage, consistent with the many studies of cation effects on anatase TiO_2. Nusbaume et al. have shown that cations influence the efficiency of dye-sensitized solar cells with non-iodide electrolytes [92]. Dye-sensitized nanocrystalline anatase TiO_2 solar cells with a $[Co(dbbip)_2]Cl_2$ redox couple were studied, where dppib is 2,6-bis(1′-butylbenzimidazol-2′-yl)pyridine. The addition of 0.1 M $LiClO_4$ to the electrolyte solution doubled the short-circuit photocurrent density and caused an ∼10% decrease of open-circuit photovoltage. These studies suggest a generality to the influence of the interfacial cation concentration on the efficiency of dye-sensitized solar cells.

Qu and Meyer recently reported a novel strategy for controlling the interfacial proton concentration at nanocrystalline TiO_2 electrodes in nonaqueous environments [73]. They pretreated TiO_2 with acidic or basic aqueous solutions prior to adsorption of ruthenium polypyridyl sensitizers. As discussed above, the acidity of the pretreatment solution determined the binding mode of the sensitizer. Acidic pretreatment caused a “carboxylic acid” binding mode, while basic pretreatment caused a “carboxylate” binding mode. Significantly higher surface coverages and stability were observed for the base-pretreated films. In addition, the aqueous pretreatment conditions exerted a profound influence on the interfacial electron transfer reactions of the sensitizer-modified films. Electron injection quantum yields, as determined by transient absorption, PL quenching, and photocurrent measurements, varied from <0.05 to ∼1, with acid-pretreated films exhibiting higher injection yields. The influence of pretreatment conditions on the injection yield was attributed to a thermodynamic effect, arising from the pH-induced shifting of TiO_2 acceptor states. These results suggest that preexposure of unmodified nanocrystalline TiO_2 films to aqueous solutions of varying pH exerts a lasting influence on the interfacial proton concentration. Interestingly, the injection yield of pH 11-pretreated, sensitizer-derivatized films could be turned on by adding $LiClO_4$ to the external acetonitrile solution. Thus, pre-exposure of unmodified TiO_2 films to aqueous solutions of varying pH exerts a similar thermodynamic effect as exposure of sensitizer-derivatized TiO_2 films to nonaqueous solutions of varying cation concentration.

Related studies of the effects of interfacial proton concentration on the photoelectrochemistry of nonaqueous solar cells were reported by Nazeeruddin and others [93,94]. They studied $Ru(dcb)_2(NCS)_2$, the “N3” dye, and its analogues with the bipyridine carboxylate groups in different protonation states. Based on ATR–FTIR measurements, they argued that the surface attachment of the complexes to anatase TiO_2 occurs through two of the four carboxylate groups in a chelating or bridging bidentate mode. The degree of protonation of the bipyridine carboxylate groups influenced the short-circuit photocurrent density and the open-circuit photovoltage, and therefore the global efficiency, of dye-sensitized solar cells. The mono-protonated form of the N3 dye exhibited the highest global efficiency, 9.3%, under simulated AM 1.5 sunlight. The influence of the dye’s protonation state on the photoelectrochemical performance was attributed to proton-induced energetic shifts of TiO_2 acceptor states.

We have outlined a number of reports of cation-dependent electron injection yields. In each case, increased excited-state electron injection yields were observed at higher interfacial cation concentration. The effect is attributed to the positive shift of TiO_2 acceptor state potentials, due to the increased positive charge at the TiO_2 surface. Cation-dependent electron injection yields have been utilized to influence the efficiencies and yields of excited-state decay processes at the TiO_2/electrolyte interface.

4.4. Influence of cations on electron injection dynamics

A key to the efficiency of nanocrystalline dye-sensitized solar cells is that electron injection is many orders of magnitude faster than charge recombination. The reason for this fortuitous difference in rate constants has been the subject of much discussion. Many femtosecond transient absorption studies of electron injection from ruthenium polypyridyl sensitizers into nanocrystalline TiO_2 films have been reported in the last decade [95–103]. Recent studies have revealed that electron injection occurs with complex, multiexponential kinetics, with an ultrafast component on a time scale <150 fs and various slower components with picosecond time scales [98–103]. Kallioinen et al. have recently reported a thorough investigation of the injection dynamics of *cis*-$Ru(dcb)_2(NCS)_2$ on nanocrystalline TiO_2 films [103]. They found that the majority of electron injection occurs from vibrationally-excited levels of the ^{1}MLCT excited state on a time scale of ∼30 fs. Injection from vibrationally-excited ^{1}MLCT states competes with rapid intersystem crossing to the ^{3}MLCT state. Following intersystem crossing, the remainder of injection occurs from the ^{3}MLCT state on time scales from 1 to 60 ps.

Several recent studies have investigated cation effects on excited-state electron injection dynamics. Durrant and coworkers reported femtosecond time-resolved near-IR absorption measurements that probed the influence of Li^+ on the dynamics of electron injection from *cis*-$Ru(dcb)_2(NCS)_2$ on nanocrystalline TiO_2 [104]. They measured in situ spectra of the *cis*-$Ru(dcb)_2(NCS)_2$-modified nanocrystalline TiO_2 working electrodes of three-electrode photoelectrochemical cells. The rise time of the absorptive signal at 800 nm, corresponding to the oxidized dye, depended on whether or not $LiClO_4$ was present in the electrolyte solution. Electron injection kinetics were multiexponential, requiring a minimum of three components to fit the data. In the presence of 0.1 M $LiClO_4$, ∼40% of electron injection occurred within 150 fs, the instrument response time. In the absence of $LiClO_4$, only ∼7.5% of injection occurred within 150 fs (Fig. 7). The lithium dependence was attributed to positive shifts of the density of TiO_2 acceptor states, $D(E)$, and increased energetic overlap with the sensitizer excited-state donor distribution function, $W_{don}(E)$ (Eq. (1)). The authors also studied the dependence of applied potential on the injection yield. Slower injection kinetics at negative applied potentials were attributed to poorer overlap of $W_{don}(E)$ with $D(E)$, due to electrochemical filling of TiO_2 acceptor states.

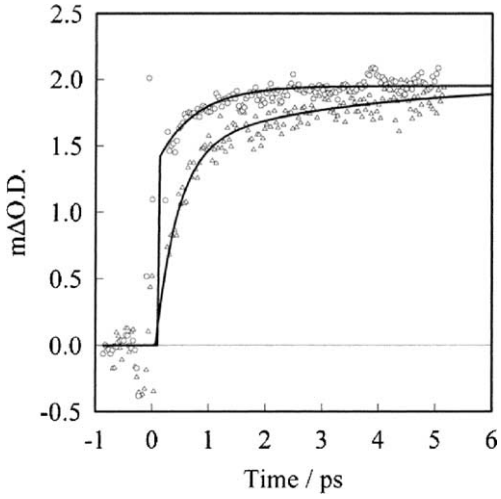

Fig. 7.

Durrant and coworkers recently reported time-resolved near-IR measurements on $(TBA)_2Ru(dcbpyH)_2(NCS)_2$ adsorbed to nanocrystalline TiO_2, where dcbpyH = 2,2′-bipyridine-4-COOH-4′-COO^- [105]. As discussed above, Grätzel and coworkers have suggested that the protonation state of the carboxylated bipyridine ligands influenced the interfacial proton concentration, and therefore the TiO_2 acceptor state energetics. The electron injection kinetics were roughly 30-fold slower for $(TBA)_2Ru(dcbpyH)_2(NCS)_2$ than for the fully-protonated dye, *cis*-$Ru(dcb)_2(NCS)_2$. The difference in injection rates was attributed to proton-induced shifting of TiO_2 acceptor state energetics.

Lian and coworkers recently reported femtosecond mid-IR transient absorption studies of pH-dependent electron injection dynamics for *cis*-$Ru(dcb)_2(NCS)_2$-modified nanocrystalline TiO_2 films [106]. Multiexponential injection kinetics were observed for films soaked in aqueous buffer solutions from pH 2 to 8 (the pH window was limited by desorption of the dye at more basic pHs). The time scale of the fast component was <100 fs and was independent of pH. The relative amplitudes of the fast and slow components varied with pH, with the contribution from the faster component decreasing at more basic pHs. This effect was attributed to the shift of TiO_2 acceptor states to more negative potentials at basic pHs, causing a decrease in the overlap of vibrationally-hot excited states with the density of semiconductor acceptor states.

The studies outlined above have revealed that electron injection dynamics are complex and multiexponential. Ultrafast injection has been attributed to electron transfer from vibrationally-excited levels of the ^{1}MLCT excited state, while injection on the picosecond time scale has been attributed to electron transfer from the ^{3}MLCT excited state. Increasing the interfacial concentration of Li^+ and H^+ apparently results in a greater yield of injection from

high-lying vibrational levels in the ^{1}MLCT excited state. This effect has been attributed to cation-induced positive shifts of TiO_2 acceptor states.

4.5. Influence of cations on the kinetics of charge recombination and iodide oxidation

The kinetics and efficiency of charge recombination and iodide oxidation are important in determining the efficiency of dye-sensitized solar cells. Charge recombination kinetics are complex and may depend on the nature and energetics of the semiconductor acceptor states and the sensitizer excited state. Charge recombination time scales ranging from picoseconds to milliseconds have been reported [7,68,76,107–112]. As we have discussed in detail, the interfacial cation concentration determines the energies of TiO_2 acceptor states. In certain cases, the relative energies of the TiO_2 acceptor states and the sensitizer ground state have been shown to influence the kinetics of charge recombination.

Several groups have investigated the driving force dependence of charge recombination following electron injection. Two strategies have been employed for controlling the driving force: variation of the sensitizer ground state reduction potential and variation of the semiconductor acceptor state potential by cation-induced shifts. Yan and Hupp studied the recombination kinetics of $Ru(dpb)_3^{2+}$ on nanocrystalline TiO_2 colloids and films, where dpb is 4,4′-$(CH_2PO(OCH_2CH_3)_2)_2$-2,2′-bipyridine [76]. Recombination kinetics were measured by time-resolving the bleach recovery at the dye's ground state MLCT absorption maximum. The phosphonic ester-derivatized complex remained adsorbed to the TiO_2 surface over 19 pH units, from $H_0 = -8$ to pH 11. Charge recombination kinetics were biphasic. Biasing the TiO_2 films negatively resulted in the elimination of the slow component, which was attributed to filling of trap states. The rate of the fast component was on the order of $10^8\,s^{-1}$, and was found to be completely independent of pH in spite of a 1.1 eV change in the driving force for recombination. Yan and Hupp attributed the surprising result to either recombination from a pH-independent surface state or proton-coupled electron transfer.

Hasselmann and Meyer have also observed driving force-independent recombination kinetics [108]. They studied the recombination reactions of nanocrystalline TiO_2 films derivatized with the Re(I) complexes *fac*-Re(deeb)$(CO)_3$(X), where X is I^-, Br^-, Cl^-, and CN^-, and *fac*-Re(deeb)$(CO)_3(py)^+$, where py is pyridine. Time-resolved absorption data were well modeled by second-order equal concentration kinetics, and recombination rates were insensitive to an ∼960 mV variation of driving force. The authors attributed the sensitizer-independent kinetics to a mechanism in which the rate of recombination is governed by diffusional encounters of electrons and holes. The rate-limiting steps in this process are electron-hopping between semiconductor trap states and hole-hopping between surface-adsorbed sensitizers through self-exchange reactions.

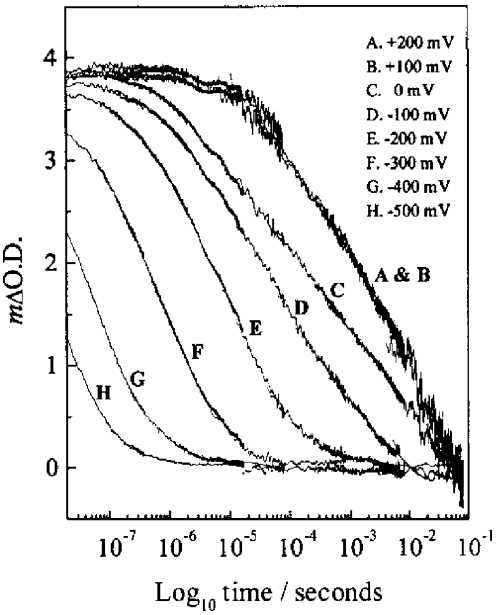

Fig. 8.

Durrant and coworkers have measured the charge recombination kinetics of *cis*-Ru$(dcb)_2(NCS)_2$-derivatized nanocrystalline TiO_2 films [109,110]. Charge recombination rates were determined from changes in the 820 nm absorption of the dye cation. The charge recombination kinetics were multiexponential and strongly dependent on applied bias, excitation intensity, and electrolyte composition. The recombination rate was found to vary over eight orders of magnitude with changes in the applied bias (Fig. 8). At positive potentials, recombination was on the milliseconds time scale. The application of increasingly negative applied biases resulted in a dramatic increase of the recombination rate. For instance, at an applied bias of −0.6 V versus Ag/AgCl, the recombination time scale was 100 ± 30 ps. The electrolyte composition and excitation intensity were found to influence the recombination kinetics. At a given applied bias, the addition of $LiClO_4$ to acetonitrile electrolytes resulted in slower charge recombination, while increased excitation intensity resulted in faster charge recombination. To explain the extraordinarily large variation of the recombination rate, Haque et al. proposed a mechanism in which charge recombination kinetics are controlled by the occupancy of TiO_2 conduction band or surface states. The electron occupancy in the semiconductor can be increased by biasing negatively, increasing the excitation intensity, or shifting the conduction band and surface state potentials positively with increased cation concentration. According to Haque et al., recombination kinetics exhibit a nonlinear dependence on the TiO_2 electron occupancy, with dramatic increases of the recombination rate with increasing occupancy. Their model is qualitatively consistent with Hasselmann and Meyer's observation that charge diffusion can be

rate-limiting. It also is consistent with the observed independence of recombination kinetics on the driving force. According to the mechanism of Haque et al., the TiO_2 electron occupancy is the most important factor in determining the recombination rate, rather than the potential difference between the electron in TiO_2 and the oxidized sensitizer.

Hupp and coworkers have recently reported the first examples of inverted region recombination kinetics. They studied the charge recombination reactions of SnO_2 colloids sensitized with electrostatically-bound inorganic dyes [111,112]. They attributed the occurrence of inverted region behavior to differences in the semiconductor electronic structure as a result of electrostatic, rather than covalent, dye attachment. For ruthenium polypyridyl complexes on SnO_2, the driving force for recombination was controlled by tuning the dye's ground state reduction potential and by pH-induced shifts of SnO_2 acceptor state potentials [111]. A three-fold decrease of the recombination rate was observed upon adjusting the pH from 7 to 11, corresponding to an ∼240 mV increase in the driving force. The recombination kinetics were temperature-dependent, suggesting that tunneling played a minor role. The inverted region behavior was attributed to recombination from conduction band electrons rather than discrete $M^{IV/III}$ states, due to the weak sensitizer-semiconductor attachment interaction. They speculated that covalent attachment of sensitizers to nanocrystalline TiO_2 results in the formation of localized redox-active $Ti^{III/IV}$ states, whereas electrostatic attachment of sensitizers to the nanocrystalline SnO_2 films does not significantly perturb the semiconductor electronic properties.

Gaal and Hupp studied the recombination kinetics of a series of ruthenium and osmium polypyridyl complexes electrostatically bound to SnO_2 [112]. The driving force for charge recombination spanned a range of 1.08 eV. Normal region, barrierless, and inverted region kinetic behavior were observed, depending on the driving force for charge recombination. The reorganization energy was estimated at ∼1.4 eV, based on the maximum of a rate versus driving force plot. The recombination rate was affected by the pH of the SnO_2 colloid. For a dye that exhibited normal region behavior, increasing the pH resulted in an accelerated recombination rate, while for a dye that exhibited inverted region behavior, increasing the pH resulted in a decelerated recombination rate. These changes are consistent with pH-induced shifts of SnO_2 acceptor state potentials and the resulting changes in the driving force for recombination. Gaal and Hupp argued that the dependence of recombination kinetics on the driving force indicates that the SnO_2 conduction band serves as the acceptor state, rather than discrete $Sn^{IV/III}$ surface states. They attributed the lack of surface state redox activity to the minimal perturbation of the SnO_2 electronic structure with electrostatic sensitizer attachment.

In summary, the kinetics of charge recombination are complex. For nanocrystalline TiO_2 derivatized with covalently-attached sensitizers, the recombination rate appears to be independent of the driving force. In these cases, the recombination rate is controlled by the occupancy of TiO_2 conduction band or surface states. Under conditions of low semiconductor electron occupancy, the recombination rate can be limited by diffusional encounters of electrons and holes. However, Hupp and coworkers' results suggest that electrostatic attachment of sensitizers can lead to driving force-dependent recombination kinetics. The kinetics of recombination appear to depend on whether the semiconductor conduction band or surface trap states are reduced by injection. Cation concentration can strongly affect recombination kinetics by influencing the occupation of the semiconductor conduction band and surface states or by altering the driving force of recombination. In both cases, the cation effects stem from the influence of the interfacial cation concentration on semiconductor energetics, as discussed in detail above.

The rate of iodide oxidation by the oxidized sensitizer is also critical in determining the efficiency of nanocrystalline dye-sensitized solar cells. Rapid reduction of the oxidized sensitizer by iodide prohibits charge recombination and promotes transport of the injected electron through the TiO_2 film. Pelet et al. have recently reported cation-dependent iodide oxidation kinetics for *cis*-$Ru(dcb)_2(NCS)_2$-derivatized nanocrystalline TiO_2 [113]. They used nanosecond transient absorption spectroscopy to time-resolve the recovery of the ground state MLCT absorption following injection. Sensitizer reduction occurred on time scales of 4 μs to several hundred microseconds. The rate of sensitizer reduction was dramatically increased by the addition of cationic species to the external propylene carbonate solution. The effect increased in the order neat propylene carbonate < 0.1 M TBAI < 0.1 M LiI < 0.1 M MgI_2. For each cation, a sharp increase in the dye regeneration rate was observed at a certain threshold concentration. Electrophoretic measurements revealed that this concentration corresponded to the transition from a negatively-charged to a positively-charged TiO_2 surface upon cation adsorption. The authors concluded that cation adsorption facilitates (I^-, I^-) ion pair formation on the TiO_2 surface, which greatly accelerates the rate of iodide oxidation to $I_2^{\bullet -}$.

5. Conclusions

Surface-adsorbed cations exert a profound influence on the efficiency of dye-sensitized solar cells. Cation effects are particularly complex and significant in nanocrystalline solar cells, because the semiconductor/electrolyte interface extends throughout the entire mesoporous semiconductor film. Central to many cation effects is the influence of the interfacial cation concentration on semiconductor energetics. The extent of cation adsorption and intercalation determines the energy of semiconductor acceptor states and in some cases the energy of the sensitizer excited state. Thus, the interfacial cation concentration affects the overlap of the sensitizer excited state distribution with the density of

semiconductor acceptor states, which in turn determines the rate and efficiency of electron injection. The interfacial cation concentration can also affect the stability of sensitizer surface attachment and the kinetics of charge transport, charge recombination, and iodide oxidation. The continuing investigation of cation effects should lead to further optimization of the efficiency of nanocrystalline dye-sensitized solar cells.

Acknowledgements

The Division of Chemical Sciences, Office of Basic Energy Sciences, Office of Energy Research, US Department of Energy is gratefully acknowledged for research support.

References

[1] H. Gerischer, Surf. Sci. 18 (1969) 97.
[2] H. Gerischer, Photochem. Photobiol. 16 (1972) 243.
[3] R. Memming, H. Tributsch, J. Phys. Chem. 75 (1971) 562.
[4] R. Memming, Photochem. Photobiol. 16 (1972) 325.
[5] M. Gleria, R. Memming, Zeitschrift fuer Physikalische Chemie (Munich) 98 (1975) 303.
[6] R. Memming, Surf. Sci. 101 (1980) 551.
[7] J. Desilvestro, M. Grätzel, L. Kavan, J. Moser, J. Am. Chem. Soc. 107 (1985) 2988.
[8] N. Vlachopoulos, P. Liska, J. Augustynski, M. Grätzel, J. Am. Chem. Soc. 110 (1988) 1216.
[9] P. Liska, N. Vlachopoulos, M.K. Nazeeruddin, P. Comte, M. Grätzel, J. Am. Chem. Soc. 110 (1988) 3638.
[10] M.A. Nazeeruddin, P. Liska, J. Moser, N. Vlachopoulos, M. Grätzel, Helv. Chim. Acta 73 (1990) 1788.
[11] B. O'Regan, M. Grätzel, Nature 353 (1991) 737.
[12] M.K. Nazeeruddin, A. Kay, I. Rodicio, R. Humphry-Baker, E. Müller, P. Liska, N. Vlachopoulos, M. Grätzel, J. Am. Chem. Soc. 115 (1993) 6382.
[13] M. Grätzel, in: R.D. McConnell (Ed.), Proceedings of the AIP Conference on Future Generation Photovoltaic Technologies, NREL, Denver, CO, 1997.
[14] M.A. Butler, D.S. Ginley, J. Electrochem. Soc. 125 (1978) 228.
[15] A.J. Nozik, Annu. Rev. Phys. Chem. 29 (1978) 189.
[16] H.O. Finklea, in: H.O. Finklea (Ed.), Semiconductor Electrodes, Elsevier, New York, 1988, p. 1.
[17] T. Watanabe, A. Fujishima, K.-I. Honda, Chem. Lett. (1974) 897.
[18] T. Watanabe, A. Fujishima, K. Honda, Bull. Chem. Soc. Jpn. 49 (1976) 355.
[19] J.M. Bolts, M.S. Wrighton, J. Phys. Chem. 80 (1976) 2641.
[20] T. Watanabe, A. Fujishima, O. Tatsuoki, K.-I. Honda, Bull. Chem. Soc. Jpn. 49 (1976) 8.
[21] W.D.K. Clark, N. Sutin, J. Am. Chem. Soc. 99 (1977) 4676.
[22] L.P. Sonntag, M.T. Spitler, J. Phys. Chem. 89 (1985) 1453.
[23] D.F. Watson, A. Marton, A.M. Stux, G.J. Meyer, J. Phys. Chem. B 107 (2003) 10971.
[24] W.J. Albery, P.N. Bartlett, J. Electrochem. Soc. 131 (1984) 316.
[25] A. Heller, in: Proceedings of the Conference on Chemical Research XXX. Advances in Electrochemistry: Photoelectrochemistry, Houston, Texas, 3–5 November 1986.
[26] G. Rothenberger, D. Fitzmaurice, M. Grätzel, J. Phys. Chem. 96 (1992) 5983.
[27] B. O'Regan, M. Grätzel, D. Fitzmaurice, Chem. Phys. Lett. 183 (1991) 89.
[28] B. O'Regan, M. Grätzel, D. Fitzmaurice, J. Phys. Chem. 95 (1991) 10525.
[29] G. Redmond, D. Fitzmaurice, J. Phys. Chem. 97 (1993) 1426.
[30] G. Redmond, A. O'Keeffe, C. Burgess, C. MacHale, D. Fitzmaurice, J. Phys. Chem. 97 (1993) 11081.
[31] B. Enright, G. Redmond, D. Fitzmaurice, J. Phys. Chem. 98 (1994) 6195.
[32] D. Fitzmaurice, Sol. Energy Mater. 32 (1994) 289.
[33] G. Boschloo, D. Fitzmaurice, J. Phys. Chem. B 103 (1999) 7860.
[34] F. Cao, G. Oskam, P.C. Searson, J.M. Stipkala, T.A. Heimer, F. Farzad, G.J. Meyer, J. Phys. Chem. 99 (1995) 11974.
[35] A.J. Bard, A.B. Bocarsly, F.-R.F. Fan, E.G. Walton, M.S. Wrighton, J. Am. Chem. Soc. 102 (1980) 3671.
[36] J.F. Dewald, Bell Syst. Technol. J. 39 (1960) 615.
[37] S.M. Sze, Physics of Semiconductor Devices, Wiley, New York, 1981.
[38] A. von Hippel, J. Kalnajs, W.B. Westphal, J. Phys. Chem. Solids 23 (1962) 779.
[39] A. Zaban, A. Meier, B.A. Gregg, J. Phys. Chem. B 101 (1997) 7985.
[40] L.A. Lyon, J.T. Hupp, J. Phys. Chem. 99 (1995) 15718.
[41] B.I. Lemon, J.T. Hupp, J. Phys. Chem. 100 (1996) 14578.
[42] B.I. Lemon, J.T. Hupp, J. Phys. Chem. B 101 (1997) 2426.
[43] L.A. Lyon, J.T. Hupp, J. Phys. Chem. B 103 (1999) 4623.
[44] S.M. Ryvkin, Photoelectric Effects in Semiconductors, New York Consultants Bureau, New York, 1964.
[45] S. Södergren, A. Hagfeldt, J. Olsson, S.-E. Lindquist, J. Phys. Chem. 98 (1994) 5552.
[46] K. Schwarzburg, F. Willig, Appl. Phys. Lett. 58 (1991) 2520.
[47] F. Cao, G. Oskam, G.J. Meyer, P.C. Searson, J. Phys. Chem. 100 (1996) 17021.
[48] N. Kopidakis, E.A. Schiff, N.G. Park, J. van de Lagemaat, A.J. Frank, J. Phys. Chem. B 104 (2000) 3930.
[49] J. van de Lagemaat, A.J. Frank, J. Phys. Chem. B 105 (2001) 11194.
[50] K.D. Benkstein, N. Kopidakis, J. van de Lagemaat, A.J. Frank, J. Phys. Chem. B 107 (2003) 7759.
[51] N. Kopidakis, K.D. Benkstein, J. van de Lagemaat, A.J. Frank, J. Phys. Chem. B 107 (2003) 11307.
[52] A. Solbrand, S. Lindström, H. Rensmo, A. Hagfeldt, S.-E. Lindquist, J. Phys. Chem. B 101 (1997) 2514.
[53] A. Solbrand, A. Henningsson, S. Södergren, S. Lindström, A. Hagfeldt, S.-E. Lindquist, J. Phys. Chem. B 103 (1999) 1078.
[54] N.W. Duffy, L.M. Peter, K.G.U. Wijayantha, Electrochem. Commun. 2 (2000) 262.
[55] N. Beermann, G. Boschloo, A. Hagfeldt, J. Photochem. Photobiol. A 152 (2002) 213.
[56] S. Nakade, S. Kambe, T. Kitamura, K. Wada, S. Yanagida, J. Phys. Chem. B 105 (2001) 9150.
[57] S. Kambe, S. Nakade, T. Kitamura, K. Wada, S. Yanagida, J. Phys. Chem. B 106 (2002) 2967.
[58] S. Kambe, S. Nakade, K. Wada, T. Kitamura, S. Yanagida, J. Mater. Chem. 12 (2002) 723.
[59] S. Nakade, Y. Saito, W. Kubo, T. Kanzaki, T. Kitamura, K. Wada, S. Yanagida, Electrochem. Commun. 5 (2003) 804.
[60] S. Nakade, Y. Saito, W. Kubo, T. Kitamura, K. Wada, S. Yanagida, J. Phys. Chem. B 107 (2003) 8607.
[61] S. Nakade, W. Kubo, Y. Saito, T. Kanzaki, T. Kitamura, K. Wada, S. Yanagida, J. Phys. Chem. B 107 (2003) 14244.
[62] L. Dloczik, O. Ileperuma, I. Lauermann, L.M. Peter, E.A. Ponomarev, G. Redmond, N.J. Shaw, I. Uhlendorf, J. Phys. Chem. B 101 (1997) 10281.
[63] N.-G. Park, J. van de Lagemaat, A.J. Frank, J. Phys. Chem. B 104 (2000) 8989.
[64] A.C. Fisher, L.M. Peter, E.A. Ponomarev, A.B. Walker, K.G.U. Wijayantha, J. Phys. Chem. B 104 (2000) 949.
[65] G. Schlichthörl, S.Y. Huang, J. Sprague, A.J. Frank, J. Phys. Chem. B 101 (1997) 8141.

[66] J. van de Lagemaat, K.D. Benkstein, A.J. Frank, J. Phys. Chem. B 105 (2001) 12433.
[67] M.J. Cass, F.L. Qiu, A.B. Walker, A.C. Fisher, L.M. Peter, J. Phys. Chem. B 107 (2003) 112.
[68] J. Moser, M. Grätzel, J. Am. Chem. Soc. 106 (1984) 6557.
[69] K. Kalyanasundaram, N. Vlachopoulos, V. Krishnan, A. Monnier, M. Grätzel, J. Phys. Chem. 91 (1987) 2342.
[70] O. Enea, J. Moser, M. Grätzel, J. Electroanal. Chem. 259 (1989) 59.
[71] T.A. Heimer, C.A. Bignozzi, G.J. Meyer, J. Phys. Chem. 97 (1993) 11987.
[72] C.A. Argazzi, C.A. Bignozzi, T.A. Heimer, F.N. Castellano, G.J. Meyer, Inorg. Chem. 33 (1994) 5741.
[73] P. Qu, G.J. Meyer, Langmuir 17 (2001) 6720.
[74] A. Zaban, S. Ferrere, J. Sprague, B.A. Gregg, J. Phys. Chem. B 101 (1997) 55.
[75] A. Zaban, S. Ferrere, B.A. Gregg, J. Phys. Chem. B 102 (1998) 452.
[76] S.G. Yan, J.T. Hupp, J. Phys. Chem. 100 (1996) 6867.
[77] Y. Liu, A. Hagfeldt, X.-R. Xiao, S.-E. Lindquist, Sol. Energy Mater. 55 (1998) 267.
[78] C.A. Kelly, F. Farzad, D.W. Thompson, J.M. Stipkala, G.J. Meyer, Langmuir 15 (1999) 7047.
[79] J.R. Lakowicz, Principles of Fluorescence Spectroscopy, second ed., Plenum Press, New York, 1999.
[80] C.A. Kelly, G.J. Meyer, Coord. Chem. Rev. 211 (2001) 295.
[81] C.A. Kelly, F. Farzad, D.W. Thompson, G.J. Meyer, Langmuir 15 (1999) 731.
[82] J. Rabani, K. Ushida, K. Yamashita, J. Stark, S. Gershuni, A. Kira, J. Phys. Chem. B 101 (1997) 3136.
[83] F. Farzad, D.W. Thompson, C.A. Kelly, G.J. Meyer, J. Am. Chem. Soc. 121 (1999) 5577.
[84] D.W. Thompson, C.A. Kelly, F. Farzad, G.J. Meyer, Langmuir 15 (1999) 650.
[85] B.V. Bergeron, G.J. Meyer, J. Phys. Chem. B 107 (2003) 245.
[86] M. Yang, D.W. Thompson, G.J. Meyer, Inorg. Chem. 39 (2000) 3738.
[87] M. Yang, D.W. Thompson, G.J. Meyer, Inorg. Chem. 41 (2002) 1254.
[88] E. Vrachnou, N. Vlachopoulos, M. Grätzel, J. Chem. Soc., Chem. Commun. (1987) 868.
[89] E. Vrachnou, N. Vlachopoulos, M. Grätzel, J. Electroanal. Chem. 258 (1989) 193.
[90] A.M. Stux, G.J. Meyer, J. Fluoresc. 12 (2002) 419.
[91] N.G. Park, S.-H. Chang, J. van de Lagemaat, K.-J. Kim, A.J. Frank, Bull. Korean Chem. Soc. 21 (2000) 985.
[92] H. Nusbaume, S.M. Zakeeruddin, J.E. Moser, M. Grätzel, Chem. Eur. J. 9 (2003) 3756.
[93] M.K. Nazeeruddin, S.M. Zakeeruddin, R. Humphry-Baker, M. Jirousek, P. Liska, N. Vlachopoulos, V. Shklover, C.-H. Fischer, M. Grätzel, Inorg. Chem. 38 (1999) 6298.
[94] M.K. Nazeeruddin, R. Humphry-Baker, P. Liska, M. Grätzel, J. Phys. Chem. B 107 (2003) 8981.
[95] J.M. Rehm, G.L. McLendon, Y. Nagasawa, K. Yoshihara, J. Moser, M. Grätzel, J. Phys. Chem. 100 (1996) 9577.
[96] H.N. Ghosh, J.B. Asbury, T. Lian, J. Phys. Chem. B 102 (1998) 6482.
[97] B. Burfeindt, T. Hannappel, W. Storck, F. Willig, J. Phys. Chem. 100 (1996) 16463.
[98] Y. Tachibana, J.E. Moser, M. Grätzel, D.R. Klug, J.R. Durrant, J. Phys. Chem. 100 (1996) 20056.
[99] T. Hannappel, B. Burfeindt, W. Storck, F. Willig, J. Phys. Chem. B 101 (1997) 6799.
[100] R.J. Ellingson, J.B. Asbury, S. Ferrere, H.N. Ghosh, J. Sprague, T. Lian, A.J. Nozik, J. Phys. Chem. B 102 (1998) 6455.
[101] J.B. Asbury, R.J. Ellingson, H.N. Ghosh, S. Ferrere, A.J. Nozik, T. Lian, J. Phys. Chem. B 103 (1999) 3110.
[102] J.B. Asbury, E. Hao, Y. Wang, H.N. Ghosh, T. Lian, J. Phys. Chem. B 105 (2001) 4545.
[103] J. Kallioinen, G. Benkö, V. Sundström, J.E.I. Korppi-Tommola, A.P. Yartsev, J. Phys. Chem. B 106 (2002) 4396.
[104] Y. Tachibana, S.A. Haque, I.P. Mercer, J.E. Moser, D.R. Klug, J.R. Durrant, J. Phys. Chem. B 105 (2001) 7424.
[105] Y. Tachibana, M.K. Nazeeruddin, M. Grätzel, D.R. Klug, J.R. Durrant, Chem. Phys. 285 (2002) 127.
[106] J.B. Asbury, N.A. Anderson, E. Hao, X. Ai, T. Lian, J. Phys. Chem. B 107 (2003) 7376.
[107] J.E. Moser, M. Grätzel, Chem. Phys. 176 (1993) 493.
[108] G.M. Hasselmann, G.J. Meyer, J. Phys. Chem. B 103 (1999) 7671.
[109] S.A. Haque, Y. Tachibana, D.R. Klug, J.R. Durrant, J. Phys. Chem. B 102 (1998) 1745.
[110] S.A. Haque, Y. Tachibana, R.L. Willis, J.E. Moser, M. Grätzel, D.R. Klug, J.R. Durrant, J. Phys. Chem. B 104 (2000) 538.
[111] X. Dang, J.T. Hupp, J. Am. Chem. Soc. 121 (1999) 8399.
[112] D.A. Gaal, J.T. Hupp, J. Am. Chem. Soc. 122 (2000) 1791.
[113] S. Pelet, J.E. Moser, M. Grätzel, J. Phys. Chem. B 104 (2000) 1791.